


# FSCN1 as a new druggable target in adrenocortical carcinoma

Carmen Ruggiero<sup>1,2</sup> | Mariangela Tamburello<sup>3</sup> | Elisa Rossini<sup>3</sup> | Silvia Zini<sup>3</sup> |  
 Nelly Durand<sup>1,2</sup> | Giulia Cantini<sup>4,5</sup> | Francesca Cioppi<sup>5,6</sup> | Constanze Hantel<sup>7,8</sup> |  
 Katja Kiseljak-Vassiliades<sup>9,10</sup> | Margaret E. Wierman<sup>9,10</sup> | Laura-Sophie Landwehr<sup>11</sup> |  
 Isabel Weigand<sup>11,12</sup> | Max Kurlbaum<sup>11</sup> | Daniela Zizioli<sup>13</sup> | Andrei Turtoi<sup>14,15</sup> |  
 Shengyu Yang<sup>16</sup> | Alfredo Berruti<sup>17</sup> | Michaela Luconi<sup>4,5</sup>  | Sandra Sigala<sup>3</sup> |  
 Enzo Lalli<sup>1,2,18</sup> 

## Correspondence

Carmen Ruggiero and Enzo Lalli, Institut de Pharmacologie Moléculaire et Cellulaire CNRS UMR 7275, 06560 Valbonne, France.

Email: [cruggiero@ipmc.cnrs.fr](mailto:cruggiero@ipmc.cnrs.fr) and [ninino@ipmc.cnrs.fr](mailto:ninino@ipmc.cnrs.fr)

## Funding information

Agence Nationale de la Recherche, Grant/Award Number: ANR20-CE14-0007; Fondation ARC pour la Recherche sur le Cancer, Grant/Award Number: PJA 20191209289; LabEx MAbImprove, Grant/Award Number: StartingGrant; INCa\_Inserm, Grant/Award Number: DGOS\_12553

## Abstract

Adrenocortical carcinoma (ACC) is a rare endocrine malignancy with a high risk of relapse and metastatic spread. The actin-bundling protein fascin (FSCN1) is overexpressed in aggressive ACC and represents a reliable prognostic indicator. FSCN1 has been shown to synergize with VAV2, a guanine nucleotide exchange factor for the Rho/Rac GTPase family, to enhance the invasion properties of ACC cancer cells. Based on those results, we investigated the effects of FSCN1 inactivation by CRISPR/Cas9 or pharmacological blockade on the invasive properties of ACC cells, both *in vitro* and in an *in vivo* metastatic ACC zebrafish model. Here, we showed that FSCN1 is a transcriptional target for  $\beta$ -catenin in H295R ACC cells and that its inactivation resulted in defects in cell attachment and proliferation. FSCN1 knock-out modulated the expression of genes involved in cytoskeleton dynamics and cell adhesion. When Steroidogenic Factor-1 (SF-1) dosage was upregulated in H295R cells, activating their invasive capacities, FSCN1 knock-out reduced the number of filopodia, lamellipodia/ruffles and focal adhesions, while decreasing cell invasion in Matrigel. Similar effects were produced by the FSCN1 inhibitor G2-044, which also diminished the invasion of other ACC cell lines expressing lower levels of FSCN1 than H295R. In the zebrafish model, metastases formation was significantly reduced in FSCN1 knock-out cells and G2-044 significantly reduced the number of metastases formed by ACC cells. Our results indicate that FSCN1 is a new druggable target for ACC and provide the rationale for future clinical trials with FSCN1 inhibitors in patients with ACC.

**Abbreviations:** ACC, adrenocortical carcinoma; Cas9, CRISPR associated protein 9; CRISPR, Clustered Regularly Interspaced Short Palindromic Repeats; FSCN1, fascin 1; GEF, guanine nucleotide exchange factor; NGS, next-generation sequencing.

For affiliations refer to page 12

This is an open access article under the terms of the [Creative Commons Attribution](https://creativecommons.org/licenses/by/4.0/) License, which permits use, distribution and reproduction in any medium, provided the original work is properly cited.

© 2023 The Authors. *International Journal of Cancer* published by John Wiley & Sons Ltd on behalf of UICC.

**KEYWORDS**

adrenocortical carcinoma, cytoskeleton, endocrine cancer

**What's new?**

Adrenocortical carcinoma (ACC), though rare, has a high risk of relapse and metastasis. Aggressive ACC overexpresses the actin-bundling protein fascin (FSCN1), and it is used as a prognostic indicator. Here, the authors investigated the effect of inactivating FSCN1 as a possible means of targeting the cancer. They found that FSCN1 inactivation reduced the invasiveness of ACC cells *in vitro* and in a zebrafish model, reduced the ability of ACC to proliferate. These results suggest FSCN1 could be a useful druggable target for controlling ACC.

**1 | INTRODUCTION**

Metastases are produced by the dissemination of cancer cells beyond their organ of origin. Their formation is a complex, multistep and overall very inefficient process; this probably explains why a long delay may exist between primary tumor formation and the detection of metastases. Overall, metastases are responsible for the largest number of cancer-related deaths.<sup>1,2</sup> A number of anticancer therapies are focused on counteracting cancer cell spreading in the body and formation of metastases. Most of those therapies are rationally designed by targeting critical factors implicated in the metastatic process.<sup>3</sup>

Adrenocortical carcinoma (ACC) is a rare endocrine malignancy with a high risk of relapse and metastatic spread.<sup>4</sup> Current treatments for ACC only have a limited efficacy in advanced-stage disease and rely upon the use of the adrenolytic agent mitotane<sup>5</sup> and combination chemotherapy in patients with progressive disease.<sup>6</sup> Even if immunotherapy has been shown to reduce tumor burden in some patients with ACC, its efficacy is not established at present.<sup>7</sup>

Activation of cytoskeleton dynamics by growth factor signaling and/or genomic alterations in cancer cells is crucial for their migration, invasion and dissemination.<sup>8</sup> One important protein regulating migration and invasion in cancer cells is fascin (FSCN1), encoded by the FSCN1 gene in chromosome 7p22.1. FSCN1 is an actin-bundling protein involved in the formation of filopodia and invadopodia.<sup>9,10</sup> It is almost absent in most normal epithelial tissues, while it is expressed at high levels in many cancers.<sup>11-14</sup> Its upregulation has been associated with poor prognosis and metastatic spread in several carcinomas, as revealed by meta-analyses and systemic reviews.<sup>13,14</sup> Small molecule compounds inhibiting FSCN1 have shown their potential to inhibit metastasis formation in animal models of several types of cancer.<sup>15-17</sup>

FSCN1 is overexpressed in ACC compared with normal adrenal tissue.<sup>18</sup> Its expression levels were significantly correlated to both shortened disease-free survival (DFS) and overall survival (OS) in three different cohorts of ACC patients<sup>19</sup> and high pre-operative circulating FSCN1 levels were predictors of recurrence.<sup>20</sup> FSCN1 has been shown to synergize with transcription factor SF-1 and the Rho/Rac guanine nucleotide exchange factor (GEF) VAV2<sup>21</sup> in enhancing the invasion properties of ACC cancer cells.<sup>19</sup> Based on those results, we investigated the effects of FSCN1 inactivation by CRISPR/Cas9 or pharmacological blockade on the invasive properties of ACC cells,

both *in vitro* and in an *in vivo* metastatic ACC model in zebrafish. Our results indicate that FSCN1 is a new druggable target for ACC and provide the rationale for future clinical trials with FSCN1 inhibitors in patients with ACC.

**2 | MATERIALS AND METHODS****2.1 | ACC patients**

Diagnosis of ACC was done on the basis of routine histopathological analysis. Tumor stage was evaluated according to the European Network for the Study of Adrenal Tumors classification.<sup>22</sup> The clinical characteristics of the patients and their tumors' genetic alterations are reported in Table S1.

**2.2 | Cell lines**

H295R (RRID:CVCL\_0458; derived from the primary tumor of a female patient with ACC) were obtained from ATCC. H295R/TR SF-1 GFP luc (a H295R subclone with Dox-inducible overexpression of the transcription factor SF-1),<sup>21</sup> MUC-1 (derived from a neck metastasis of a male patient with ACC),<sup>23</sup> CU-ACC2 (RRID:CVCL\_RQ01; derived from a liver metastasis of a female patient with ACC)<sup>24</sup> and JIL-2266 cells (derived from the primary tumor of a female patient with ACC)<sup>25</sup> were generated and cultured as described.<sup>21,23-25</sup> All cell lines were authenticated using STR profiling within the last 3 years and all experiments were performed with mycoplasma-free cells.

**2.3 | Establishment of CRISPR/Cas9 FSCN1 gene inactivation in human ACC H295R/TR SF-1 GFP luc cells**

H295R/TR SF-1 GFP luc cells were infected with lentivirus produced using Lenti CRISPRv2 (Addgene\_52961) bearing either a FSCN1 (GAAGAAGCAGATCTGGACGC)<sup>26</sup> or a control (CTTCCGCGGCCGTTCAA)<sup>27</sup> sgRNA and selected with puromycin. A total of four clones, two control (ctrl #1 and ctrl #2) and two FSCN1 knock-out (KO) (FSCN1

KO #1 and *FSCN1* KO #2), were selected for further studies. They were cultured in DMEM-F12 (Invitrogen) supplemented with penicillin-streptomycin, 2% NuSerum (BD), 1% ITS+ (BD) and blasticidin (5 µg/ml)-zeocin (100 µg/ml) (both from Cayla InvivoGen). To identify the mutations caused by CRISPR/Cas9 gene editing in the region targeted by the sgRNA against *FSCN1*, genomic DNA from *FSCN1* KO clones was extracted by the GenElute Mammalian Genomic DNA Miniprep kit (Sigma-Aldrich) and amplified by PCR using primers 5'-GCAGCCGAACAAAGGAGCAG-CAGG-3' (forward) and 5'-CGTCGTCGTGCGCCACGATGAGG-3' (reverse). The PCR products were then sequenced to confirm the presence of mutations. Potential off-target mutations induced by the *FSCN1* sgRNA were predicted by the use of the in silico tools CCTop (<https://cctop.cos.uni-heidelberg.de:8043>), COSMID (<https://crispr.bme.gatech.edu>), CRISPOR (<http://crispor.tefor.net>) and Off-Spotter (<https://cm.jefferson.edu/Off-Spotter>). On the basis of those analyses a list of the top 20 potential exonic off-target sites was established (Table S2). To verify the absence of mutations in those sites, genomic DNA was extracted from *FSCN1* KO clones (see above) and amplified by PCR, then PCR products were sequenced. No off-target mutation in those sites was present. Absence of *FSCN1* expression in the KO clones was confirmed by immunoblotting.

## 2.4 | Immunoblots

Immunoblots were performed as previously described.<sup>21</sup> Primary antibodies were anti-FSCN1 mouse monoclonal (sc-46 675, Santa Cruz Biotechnology; 1:1000), rabbit polyclonal anti-SF-1 (07-618, Millipore; 1:1000) and mouse monoclonal anti-GAPDH (CB1001, Sigma-Aldrich; 1:2000) antibodies. Secondary antibodies were HRP-conjugated anti-mouse (NA-931, GE Healthcare; 1:5000) and anti-rabbit (NA-934, GE Healthcare; 1:5000) antibodies. *FSCN1* and SF-1 band intensities were quantified by the Image J software (<https://imagej.net/ij>) after GAPDH normalization.

## 2.5 | Transwell invasion assay through Matrigel

It was performed as previously described.<sup>21</sup> Cells were treated with vehicle (ethanol) or doxycycline (Dox; 1 µg/ml), alone or in combination with the G2 compound (Xcessbio Biosciences; 50 µM in DMSO) or with G2-044, G2-011 or G2-112 (ValueTek; 5 µM in DMSO). CU-ACC2, JIL-2266 and MUC-1 cells were treated with vehicle (DMSO) or G2-044 (5 µM).

## 2.6 | Proliferation and cell cycle analysis

Cell proliferation was evaluated by cell counting using a Countess 3 automatic cell counter (Thermo Fisher). Doubling times were calculated using the formula:

$$\text{Doubling time} = \frac{\text{Duration} * \log(2)}{\log(\text{Final number}) - \log(\text{Initial number})}$$

Cell cycle analysis was performed by flow cytometry on ethanol-fixed, propidium iodide-stained ctrl (clones #1 and #2, each one in duplicate) and *FSCN1* KO H295R cells (clones #1 and #2, each one in duplicate) on a LSRII Fortessa (Becton Dickinson) FACS instrument. 20,000 events were acquired per sample. After electronic gating out of doublets, apoptosis was measured as the percentage of sub-G1 cells and proliferation index was calculated as the sum of the percentages of cells in the S and G2M phases of the cell cycle.

## 2.7 | Cell spreading assay

Control and *FSCN1* KO H295R cells were seeded in 24-well plates (#353047, Falcon) in triplicate wells (50,000 cells/well). After 48 h, cells were fixed by 4% paraformaldehyde for 15 min at room temperature and washed twice with PBS. Cell images were acquired with a Zeiss Axioplan 2 microscope using a ×20 objective and avoiding overlapping fields. Quantitative data analysis was performed by counting the number of spread and unspread cells per field. Eight fields per cellular clone per replicate were quantified for a number of cells between 400 and 700. Round and refringent cells were considered unspread, while dark cells with cytoplasm surrounding the entire circumference of the nucleus were considered spread. The percentage of spread or unspread cells to total cells was calculated.

## 2.8 | Immunofluorescence, filopodia, lamellipodia-ruffles, focal adhesions detection and quantification

Control and *FSCN1* KO H295R cells were treated with Dox (1 µg/ml) or vehicle for 72 h and processed for immunofluorescence as described.<sup>21</sup> Cells were incubated with mouse monoclonal anti-paxillin antibody (610 052, BD Biosciences; 1:1000), washed and incubated with Alexa 488-conjugated anti-mouse secondary antibody (A-11001, Invitrogen; 1:200). To visualize F-actin, cells were incubated with Alexa Fluor 594 phalloidin (A12381, Invitrogen; 1:400). Images were acquired with a Zeiss Axioplan 2 fluorescence microscope coupled to a digital CCD camera, processed and analyzed using ImageJ. Cell sampling was performed randomly, scoring more than 250 cells per condition per experiment to count the number of filopodia or lamellipodia/ruffles per cell. Filopodia were defined as thin, tubular, fingerlike cell protrusions filled with straight bundled cross-linked actin filaments. Lamellipodia were defined as sheet-like protrusive structures extending from the cell edge and consisting mostly of dynamic, criss-crossed actin filaments, with ruffles being of similar morphology but not adhered and moving centripetally toward the main cell body. Quantification of focal adhesion size and number was performed by

application of a threshold to all images using ImageJ to isolate and identify focal adhesions between 1 and 5  $\mu\text{m}$  in size, as previously described.<sup>28</sup> Focal adhesion size was normalized to the total cell area and showed as the percentage of the cell occupied by focal adhesions. In all analyses, at least 90 cells were evaluated. All samples were processed equally and evaluated blindly regarding sample identity.

## 2.9 | Reverse transcription quantitative polymerase chain reaction

It was performed as described<sup>21</sup> using TATA-binding protein (*TBP*) as a reference transcript. Primer sequences were as follows: *TBP*, 5'-GAA CAT CAT GGA TCA GAA CAA CA-3' (forward) and 5'-ATT GGT GTT CTG AAT AGG CTG TG-3' (reverse); *FSCN1*, 5'-ACG GCA ACG TGA CCT GCG AG-3' (forward) and 5'-GAC TGC AGC GAC CAG CGA CC-3'; *AXIN2*, 5'-ATG ATT CCA TGT CCA TGA CG-3' (forward) and 5'-CTT CAC ACT GCG ATG CAT TT-3' (reverse); *TCF7*, 5'-GGC TTC TAC TCC CTG ACC TC-3' (forward) and 5'-TGC TTG TGT CTT CAG GTT GC-3' (reverse); *SCIN*, 5'-GCA GAG TAT GTA GCA AGT GTC CT-3' (forward) and 5'-GTA AAG CCG AGG TGG ATG GTC T-3' (reverse); *VSNL1*, 5'-TTC GTT AAG TGA CCG TGC G-3' (forward) and 5'-CAT CAC TTC AGG GGC CAG TT-3' (reverse). In some experiments, H295R cells were treated with the beta-catenin inhibitor PNU-74656 (#3534, Tocris) for 24 h at a concentration of 100  $\mu\text{M}$ . This is a lower dose than the IC50 reported for this drug in the H295R cell line (129.8  $\mu\text{M}$ )<sup>29</sup> and was previously shown to efficiently inhibit beta-catenin-dependent proliferation and target gene expression in those cells.<sup>29</sup> Results were calculated using the  $\Delta\Delta\text{C}_T$  threshold cycle method.<sup>30</sup> RNA isolated from tumor tissues was subjected to RT-qPCR for the *FSCN1* and *GAPDH* transcripts using Taqman gene expression assay Hs0060251\_m1, FAM-MGB 4325934-1 301 038 (Applied Biosystems). The amount of target, normalized to the endogenous reference gene *GAPDH* and relative to a calibrator (Agilent), was calculated by the  $\Delta\Delta\text{C}_T$  method.<sup>29</sup>

## 2.10 | Transient transfection assay

H295R cells were plated in 96-well plates (20,000 cells/well) in complete culture medium. The day after the cells were co-transfected using Lipofectamine 3000 (Invitrogen), according to the manufacturer's instructions, with 100 ng of the *FSCN1* promoter luciferase reporter pmFascin-luc<sup>31</sup> (a kind gift of D. Vignjevic) or the  $\beta$ -catenin reporter TOPFLASH (21-170, Merck) and 1 ng of the *Renilla* luciferase reporter phRL-CMV. Some samples were cotransfected with pmFascin-luc (50 ng) or TOPFLASH (50 ng) plus a dominant-negative  $\Delta\text{N}$ -TCF4 expression vector (50 ng; a kind gift of D. Vignjevic) or the same quantity of empty pcDNA3.1 (Invitrogen). The day after transfection, some samples were treated with PNU-74656 (100  $\mu\text{M}$ ). After 24 h of treatment, luciferase assays were performed using a GloMax luminometer (Promega). Results were normalized by the *Renilla* signal for the pmFascin luc - transfected cells. As we realized that *Renilla*

activity in TOPFLASH transfected cells was affected by the activation status of the beta catenin pathway, those results were normalized by protein content measured by the DC Protein Assay (BioRad).

## 2.11 | Steroid hormone profiling

Control and *FSCN1* KO H295R cells were treated for 24 h with vehicle or forskolin (FSK, 10  $\mu\text{g}/\text{ml}$ ). At the end of the treatment the supernatants were collected and steroid hormone profiling was carried out by LC-MS/MS. Samples were precleaned by off-line solid-phase extraction and analytes were separated by an Agilent 1290 UHPLC system. Steroids were measured in MRM mode with an QTRAP 6500+ (Sciex, Framingham) mass spectrometer. Details are described elsewhere.<sup>32</sup>

## 2.12 | RNA-sequencing

For RNA-seq, duplicates of each H295R clone (ctrl #1 and 2 and *FSCN1* KO #1 and 2) were processed. Total RNA was extracted by Trizol reagent (Invitrogen). RNA concentrations were measured and quality assessed by Agilent 2100 Bioanalyzer (Agilent Technologies). Samples were subjected to DNase treatment using the TURBO DNA-free kit (Invitrogen) and rRNA depleted by the RiboZero kit (Illumina). Libraries were prepared according to the manufacturer's protocol (Illumina) and sequenced on a NovaSeq instrument at  $2 \times 150$  bp paired reads. The sequencing coverage and quality statistics for each sample are summarized in Table S3. Data analysis steps were performed on the Galaxy web platform.<sup>33</sup> The FastQC tool was used for quality control of raw fastq data. Only reads with quality value >30 were further processed. Adapter sequences were removed by Trimmomatic and reads were mapped on the human genome (hg38) using RNA STAR. The number of reads mapping to NCBI RefSeq features were calculated by the featureCounts tool with parameters: stranded, reverse; minimum mapping quality, 10; feature type, exon. Counts were normalized using the DESeq2 tool. Differentially expressed genes (DEG) were identified using the iDEP.96 web tool (<http://bioinformatics.sdstate.edu/idep96>) as regulated >2-fold with a P-value <0.1. DEG were annotated using Metascape<sup>34</sup> and plotted using the SRplot web tool (<http://www.bioinformatics.com.cn/srplot>).

## 2.13 | Proteomics

For proteomic analysis, duplicates of each H295R clone (ctrl #1 and 2 and *FSCN1* KO #1 and 2) were processed. 100  $\mu\text{g}$  protein per sample was digested with trypsin (2  $\mu\text{g}$ ). Peptides were labeled with TMTPro 16Plex (Thermo Fisher) and pooled. The labeled peptide samples were fractionated in reverse phase into seven fractions using a nano-flow HPLC (RSLC U3000, Thermo Fisher) coupled to a mass spectrometer equipped with a nanoelectrospray source and FAIMS technology (Exploris 480, Thermo Fisher). The spectra were recorded via Xcalibur 4.2 software (Thermo Fisher) and data were analyzed

using Proteome Discoverer 2.4 and Perseus v1.6.10.43, with the use of Masterleading FPP v3.4ML1. Data validation was performed with the following filters: peptide FDR 0.01 and protein FDR 0.05 (high confidence: 0.01 and medium: 0.05). Venn diagrams were drawn using jvenn.<sup>35</sup>

## 2.14 | Metabolomics

Untargeted metabolomic analysis was performed on duplicates of each H295R clone (control #1 and 2 and *FSCN1* KO #1 and 2). One million cells were pelleted at 200g for 10 min and extracted with a methanol-water mix (3:1, v/v) containing 1% formic acid. The homogenate was then centrifuged at 15000g at 4°C for 15 min and the supernatant was loaded on the Captiva EMR plate (5190-1001, Agilent) assembled on the Vacuum Manifold (A796, Agilent) together with the Deep Well collection plate (A696001000, Agilent). The flow-through was collected and dried using lyophilization. Prior to analysis, samples were diluted in 200  $\mu$ l water and 1  $\mu$ l was injected on a LC-MS system consisting of UHPLC (Vanquish Flex, Thermo Fisher) coupled to orbitrap MS (QExactive Plus, Thermo Fisher). The MS acquisition method was data dependent, where top 5 MS ions with default charge of 1 were selected for MS/MS fragmentation. Two acquisitions were conducted for each sample, one in positive and one in negative mode. Raw data were then imported in Compound Discoverer (CD) software (Version 3.3, Thermo Fisher) where they were processed using the default untargeted metabolomics workflow. Statistical analysis of modulated metabolites was performed using the CD software, where a *P* value <.05 was considered as significant.

## 2.15 | Cancer cell xenografts in zebrafish

The adult transgenic zebrafish (*Danio rerio*) line Tg(kdrl:EGFP) was maintained as described.<sup>36</sup> Breeding of adult male and female zebrafish was carried out by natural crosses, and embryos were collected and raised in fish water with incubation at 28.5°C until the experiments. Embryos at 24 h post-fertilization (hpf) were treated with 0.003% 1-phenyl-2-thiourea (PTU) to prevent pigmentation. After the completion of the experiments, zebrafish embryos were euthanized with 400 mg/L tricaine (ethyl 3-aminobenzoate methane sulfonate salt; Sigma-Aldrich).

Xenografts of vehicle-treated and Dox-treated (1  $\mu$ g/ml) control and *FSCN1* KO were realized as previously described.<sup>37</sup> Briefly, Tg(kdrl:EGFP) zebrafish embryos at 48 hpf were dechorionated, anesthetized with 0.042 mg/ml tricaine and microinjected with the labeled cells (CellTracker™ CM-Dil Dye, Thermo Fisher) into the subperidermal space of the yolk sac. Microinjections were performed with a FemtoJet electronic microinjector coupled with an InjectMan N12 manipulator (Eppendorf). Approximately 250 cells/4 nl were injected into each embryo (about 100 embryos/group); embryos were maintained in PTU/fish water in a 32°C incubator to allow tumor cell growth. To investigate the effects on metastasis formation, 1  $\mu$ g/ml

Dox was directly added to the PTU/fish water. To assess the effect of *FSCN1* pharmacological inhibition, embryos xenografted with Dox-pretreated control cells were placed in the PTU/fish water spiked with 1  $\mu$ g/ml Dox and G2-044 (at the concentration of 2.5 or 5  $\mu$ M) or vehicle. Images of injected embryos were acquired using an Axiozoom V13 fluorescence microscope (Zeiss), equipped with Zen pro software. After 3 days, embryos with metastases (defined as the presence of at least one fluorescent spot outside the site of injection) were counted. Some representative xenografted embryos with metastasis were fixed, embedded in low melting agarose and images acquired with a LSM 510 confocal laser microscope equipped with an Achroplan  $\times$ 10/0.25 objective. Images were then reconstructed using Zen 2.3 Black software (Zeiss).

## 2.16 | Statistical analyses

They were performed using GraphPad Prism software version 9.4, considering a *P* value <.05 as the threshold for a significant difference.

# 3 | RESULTS

## 3.1 | *FSCN1* expression is regulated by $\beta$ -catenin in H295R ACC cells and correlates with *CTNNB1*/ $\beta$ -catenin pathway gene mutations and the expression of $\beta$ -catenin target genes in ACC

*FSCN1* is overexpressed in aggressive ACC, being a reliable prognostic indicator in this cancer type.<sup>19,20</sup> Somatic mutations of *CTNNB1*, encoding  $\beta$ -catenin or other genes leading to constitutive activation of the canonical Wnt pathway are present in about 1/3 of ACC, alone or in combination with other genomic alterations.<sup>38</sup> Similar to *FSCN1* overexpression,  $\beta$ -catenin activation is associated to poor outcome in ACC.<sup>39</sup>  $\beta$ -catenin was reported to regulate transcriptionally *FSCN1* expression in colon cancer cells.<sup>31</sup> H295R cells, the most widely used human ACC cell line, bear an activating mutation in *CTNNB1*<sup>40</sup> and express high levels of *FSCN1*.<sup>19</sup> We then investigated whether *FSCN1* is a transcriptional target for  $\beta$ -catenin in H295R cells. The small compound PNU-74654, an inhibitor of the interaction of  $\beta$ -catenin with Tcf transcription factors, significantly down-regulated *FSCN1* expression as well as the known  $\beta$ -catenin target genes *AXIN2* and *TCF7* (Figure 1A). Consistent with those findings, both PNU-74654 and a cotransfected dominant-negative TCF4 ( $\Delta$ N-TCF4) significantly repressed expression of a *FSCN1* promoter-luciferase reporter<sup>31</sup> as well as the canonical  $\beta$ -catenin-responsive TOPFLASH reporter in H295R cells (Figure 1B). Consistent with these results, in a cohort of ACC from the Florence University hospital, tumors harboring *CTNNB1* activating mutations had significantly higher *FSCN1* mRNA levels than tumors without *CTNNB1* mutations (Figure 1C). In the TCGA ACC cohort, *FSCN1* mRNA levels were significantly higher in tumors bearing activating *CTNNB1* mutations (Figure 1D) or also bearing alterations in other beta-catenin pathway genes (*APC* mutations and

ZNR3 deletions/mutations) in addition to CTNNB1 compared with tumors without genomic alterations in that pathway (Figure 1E). Moreover, in the TCGA ACC cohort, FSCN1 mRNA levels are

positively correlated with CTNNB1 levels and with the expression levels of several bona fide  $\beta$ -catenin target genes in ACC (AXIN2, LEF1, AFF3, FAM194A, ISM1, PXYLP1 and NKD1)<sup>41</sup> (Figure 1F).

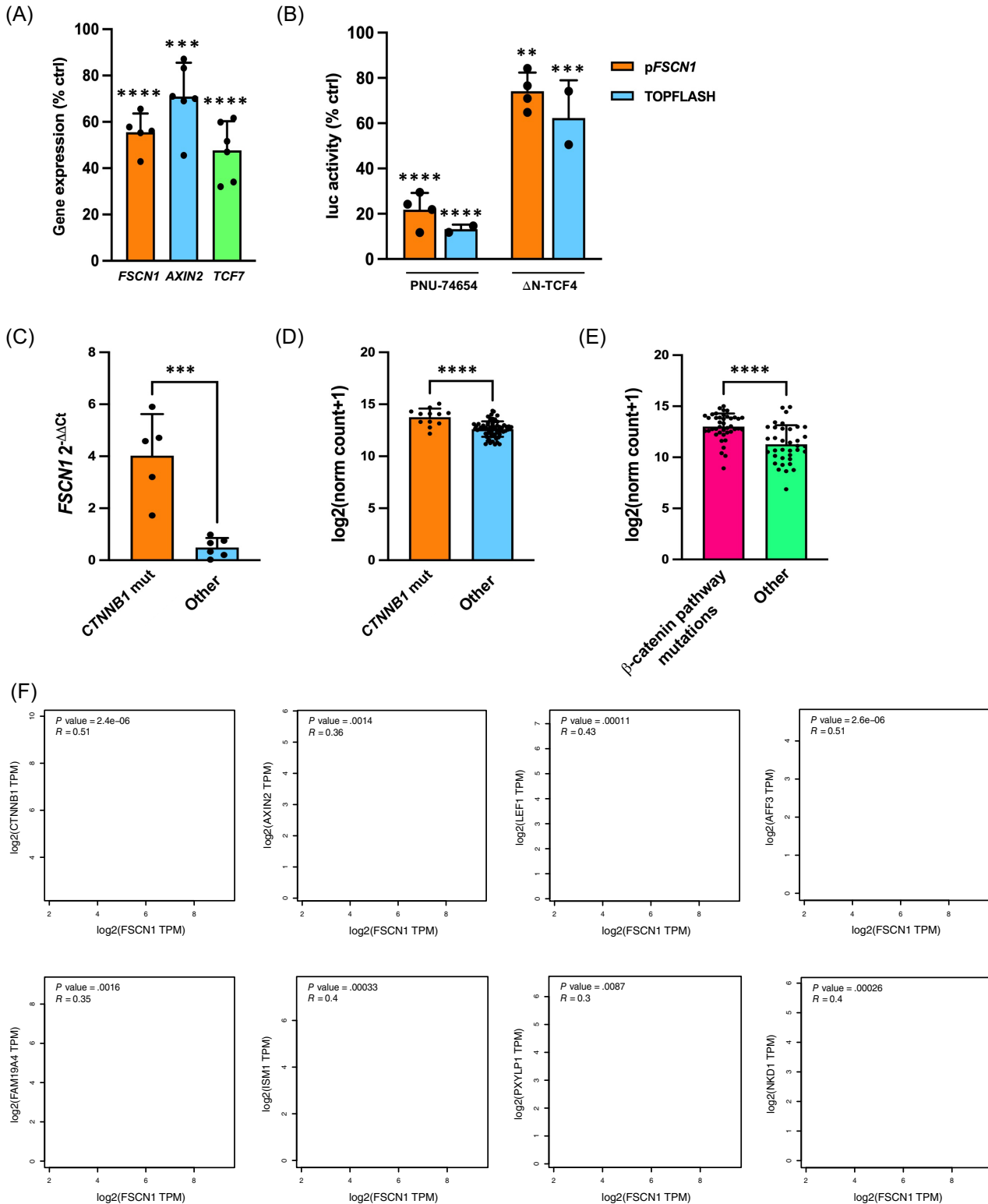


FIGURE 1 Legend on next page.

### 3.2 | *FSCN1* inactivation in ACC cells induces defects in cell attachment to substrate and proliferation

To study the role of *FSCN1* in an ACC cell model, several H295R cell clones were produced where *FSCN1* was inactivated by CRISPR/Cas 9 recombination. To be able to study the effect of *FSCN1* inactivation on biological effects caused by overexpression of the transcription factor SF-1, the H295R/TR SF-1 GFP luc subclone was used to perform *FSCN1* knockout (KO), where SF-1 dosage can be increased by Dox treatment.<sup>19,21</sup> Two cell clones with successfully targeted *FSCN1* and two clones transfected with a control sgRNA were selected at random for further experiments (Figure 2A). We verified the absence of recombination in potential off-target sequences in the *FSCN1* KO clones (Table S2). *FSCN1* inactivation did not produce noticeable effects on cell cytoskeleton architecture, as visualized by phalloidin and paxillin staining (Figures 2B and S1). However, *FSCN1* KO cells showed impaired attachment to the culture substrate and decreased spreading after plating compared with the control clones (Figures 2C and S2). *FSCN1* KO cells also showed a proliferation defect compared with the control clones (doubling time of control clone #1:58.96 h; control clone #2:55.13 h; *FSCN1* KO clone #1:65.96 h; *FSCN1* KO clone #2:84.01 h) (Figures 2D and S3). Flow cytometric analysis showed that the proliferation index (S + G2/M) was higher in ctrl (27.83%) compared with *FSCN1* KO cells (24.95%), while the percentage of apoptotic (sub-G1) cells was slightly higher in *FSCN1* KO cells (1.37%) compared with ctrl cells (1%) (Figure S4 and Table S4).

### 3.3 | Effects of *FSCN1* inactivation on steroidogenesis, gene and protein expression, and metabolic profiles in ACC cells

H295R cells are a differentiated ACC cell line producing a large variety of steroids.<sup>32,40</sup> Since cytoskeletal dynamics are known to affect steroid production in adrenocortical cells,<sup>42</sup> we compared the concentrations of several steroids in the culture medium in control and *FSCN1* KO cells, both in basal conditions and after stimulation with FSK, a pharmacological activator of adenylate cyclase. *FSCN1* inactivation

had no effect on steroid production, both in basal conditions (Table S5) or after stimulation with FSK (Figure S5).

To assess the impact of *FSCN1* inactivation on global gene and protein expression in H295R cells, we performed RNA-seq and proteomic profiling of control and *FSCN1* KO clones. A distinct set of genes was differentially expressed in *FSCN1* KO cells compared with control (Figure 3A and Table S6). Pathways related to cell architecture and motility were significantly enriched among those DEG (Figure 3B). In proteomic analysis, only seven proteins were found to be differentially expressed in *FSCN1* KO cells compared with control (Table S7). Among those, adseverin/scinderin (SCIN) and visinin-like 1 (VSNL1) were consistently upregulated in *FSCN1* KO cells, both at the transcript and protein levels (Figure 3A, C and Tables S6 and S7). *SCIN* and *VSNL1* mRNA upregulation in *FSCN1* KO cells was confirmed by RT-qPCR (Figure 3D).

*FSCN1* has been recently associated to the control of oxidative phosphorylation through regulation of the mitochondrial actin cytoskeleton.<sup>26</sup> To evaluate the impact of *FSCN1* inactivation on global metabolic profiles in H295R cells, we performed untargeted metabolomics and identified a set of metabolites which were all depleted in *FSCN1* KO compared with control cells (Table S8). Those included aspartic-glutamic acid and some pyrimidines.

### 3.4 | Inactivation of *FSCN1* expression or pharmacological antagonism in ACC cells induces defects in Matrigel invasion in vitro

Overexpression of transcription factor SF-1 is a marker of malignancy in ACC.<sup>43</sup> An increased SF-1 dosage in the H295R cell line considerably increases their invasive properties *in vitro* and *in vivo*.<sup>19,21</sup> We have previously shown that *FSCN1* knockdown or treatment with the *FSCN1* small molecule inhibitor G2 impaired Matrigel invasion of H295R cells triggered by SF-1 overexpression.<sup>19</sup> We then investigated the effects of *FSCN1* gene inactivation on the invasive behavior of H295R cells *in vitro*. No differences were present in the number of filopodia (Figure 4A), lamellipodia/ruffles (Figure 4B) and focal adhesions (Figure 4C) between control and *FSCN1* KO cells in basal culture conditions. However, treatment with Dox, which increases SF-1

**FIGURE 1** *FSCN1* expression is linked to  $\beta$ -catenin activation in ACC. (A) The  $\beta$ -catenin inhibitor PNU-74654 inhibits expression of *FSCN1*, *AXIN2* and *TCF7* in H295R cells. Cells were treated with drug (100  $\mu$ M) or vehicle for 24 h, then gene expression was measured by RT-qPCR. Results are shown as percentage of expression compared with vehicle-treated cells.  $n$  (independent experiments) = 5–6. Mean  $\pm$  SD is shown. \*\*\* $P$  < .001; \*\*\*\* $P$  < .0001, one-way ANOVA with Šidák's multiple comparisons test. (B) The *FSCN1* promoter is repressed by inhibition of  $\beta$ -catenin transcriptional activity in H295R cells. Cells were transfected with *FSCN1* promoter-luciferase reporter (p*FSCN1*) or the control  $\beta$ -catenin-responsive TOPFLASH reporter. To inhibit  $\beta$ -catenin, cells were either treated with PNU-74654 (100  $\mu$ M) or cotransfected with a dominant-negative TCF4 ( $\Delta$ N-TCF4) expression plasmid. Results are shown as percentage of luciferase activity compared with vehicle-treated cells (PNU-74654) or empty expression vector ( $\Delta$ N-TCF4).  $n$  (independent experiments) = 2–4. Mean  $\pm$  SD is shown. \*\* $P$  < .01; \*\*\* $P$  < .001; \*\*\*\* $P$  < .0001, one-way ANOVA with Šidák's multiple comparisons test. (C) Higher *FSCN1* mRNA levels in *CTNNB1*-mutated ACC than in tumors without *CTNNB1* mutations in the Florence cohort;  $n$  (patients number) = 11. Mean  $\pm$  SD is shown. \*\*\* $P$  < .001,  $t$ -test. (D) Higher *FSCN1* mRNA levels in *CTNNB1*-mutated and (E) beta-catenin pathway (*APC*, *ZNRF3*, *CTNNB1*)-mutated ACC compared with other tumors in the TCGA cohort;  $n$  (patients number) = 78. Mean  $\pm$  SD is shown. \*\*\*\* $P$  < .0001,  $t$  test. Data were retrieved and analyzed using Xena (<https://xenabrowser.net>). (F) Positive correlation of expression between *FSCN1*-*CTNNB1* and  $\beta$ -catenin target genes *AXIN2*, *LEF1*, *AFF3*, *FAM194A*, *ISM1*, *PXYLP1* and *NKD1* in ACC from the TCGA cohort. Data were retrieved and analyzed using GEPIA (<http://gepia.cancer-pku.cn/detail.php?clicktag=correlation>). [Color figure can be viewed at [wileyonlinelibrary.com](http://wileyonlinelibrary.com)]

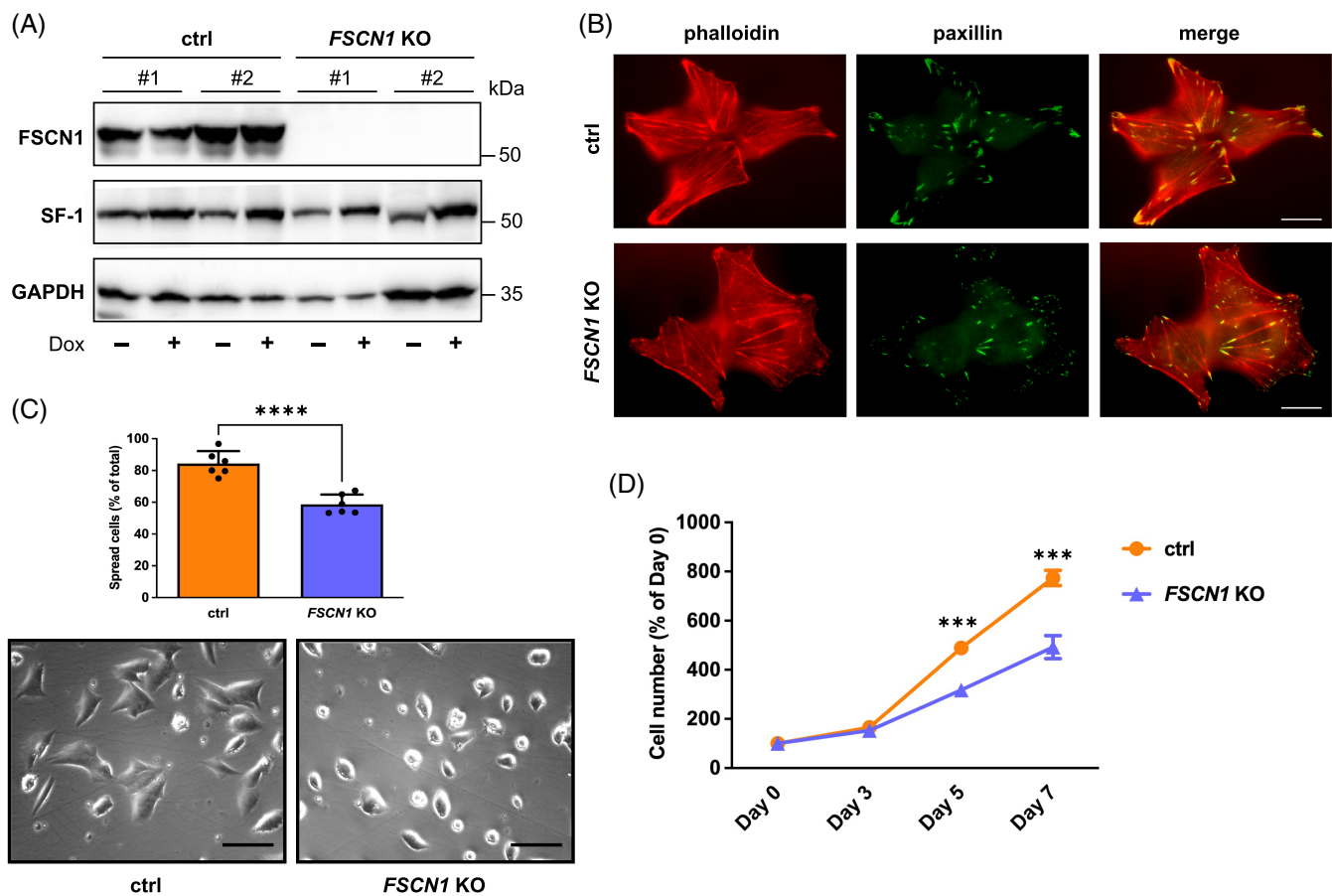


**FIGURE 2** FSCN1 inactivation in H295R cells causes defects in spreading after plating and proliferation. (A) Western blot showing expression of FSCN1, SF-1 and GAPDH in control #1 and #2 and in FSCN1 KO #1 and #2 H295R clones in basal conditions and after treatment with Dox (1  $\mu$ g/ml) for 72 h. (B) Staining of control and FSCN1 KO cells with phalloidin (actin cytoskeleton; in red) and paxillin (focal adhesions; in green). Scale bar, 5  $\mu$ m. (C) FSCN1 KO cells have a spreading defect after plating. The histogram shows the percentage of spread cells 48 h after plating for control and FSCN1 KO H295R cells. Data are derived from the combined analysis of control #1 and #2 (orange) and FSCN1 KO #1 and #2 H295R clones (violet). Data for individual clones are shown in Figure S1.  $n$  (independent experiments) = 6. Mean  $\pm$  SD is shown. \*\*\*\* $P$  < 0.0001,  $t$  test. Bottom: Representative micrographs of control and FSCN1 KO cells taken 48 h after plating. Scale bar, 20  $\mu$ m. (D) FSCN1 KO cells proliferation is slower compared with control cells. Data are derived from the combined analysis of control #1 and #2 (orange line) and FSCN1 KO #1 and #2 H295R clones (violet line). Cells were cultured without adding Dox in the culture medium. Data for individual clones are shown in Figure S3.  $n$  (independent experiments) = 6. Mean  $\pm$  SD is shown. \*\*\* $P$  < .001,  $t$  test. [Color figure can be viewed at [wileyonlinelibrary.com](http://wileyonlinelibrary.com)]

expression (Figure 2A), induced no significant increases in the number of those cytoskeletal structures in FSCN1 KO cells, in contrast to control cells (Figure 4A-C). Consistent with those data, SF-1 dosage-dependent invasion through Matrigel was significantly impaired in FSCN1 KO cells compared with control cells (Figure 4D). A series of small molecule FSCN1 inhibitors has been developed recently, which have improved potency compared with the first inhibitor described, G2.<sup>17</sup> G2 at the concentration of 50  $\mu$ M, and its derivatives G2-044 and G2-011 at the concentration of 5  $\mu$ M significantly inhibited Matrigel invasion of Dox-treated H295R/TR SF-1 cells. Conversely, the similar but inactive compound G2-012 (5  $\mu$ M) had no effect (Figure 4E). In addition to H295R, a few new differentiated ACC cell lines have been produced recently.<sup>22-24</sup> Those cell lines express variable levels of FSCN1, with H295R showing the highest and MUC-1 the lowest expression. H295R cells also express the highest levels of SF-1, followed by MUC-1,

CU-ACC2 and JIL-2266 (Figure 4F). Similar to its effect in H295R cells, the G2-044 compound significantly inhibited Matrigel invasion in all the other ACC cell lines tested (Figure 4G). Treatment with G2-044 had no effect on SCIN expression in CU-ACC2, JIL-2266 and MUC-1 cells and slightly increased expression of VSNL-1 only in CU-ACC2 cells (Figure S6).

### 3.5 | Inactivation of FSCN1 expression or its pharmacological inhibition in ACC cells induces defects in *in vivo* invasion in a zebrafish metastatic tumor model

A zebrafish model<sup>37</sup> was used to assay the effect of both FSCN1 inactivation and pharmacological inhibition on the metastatic behavior of H295R cells stimulated by an increased SF-1 dosage. Zebrafish do not



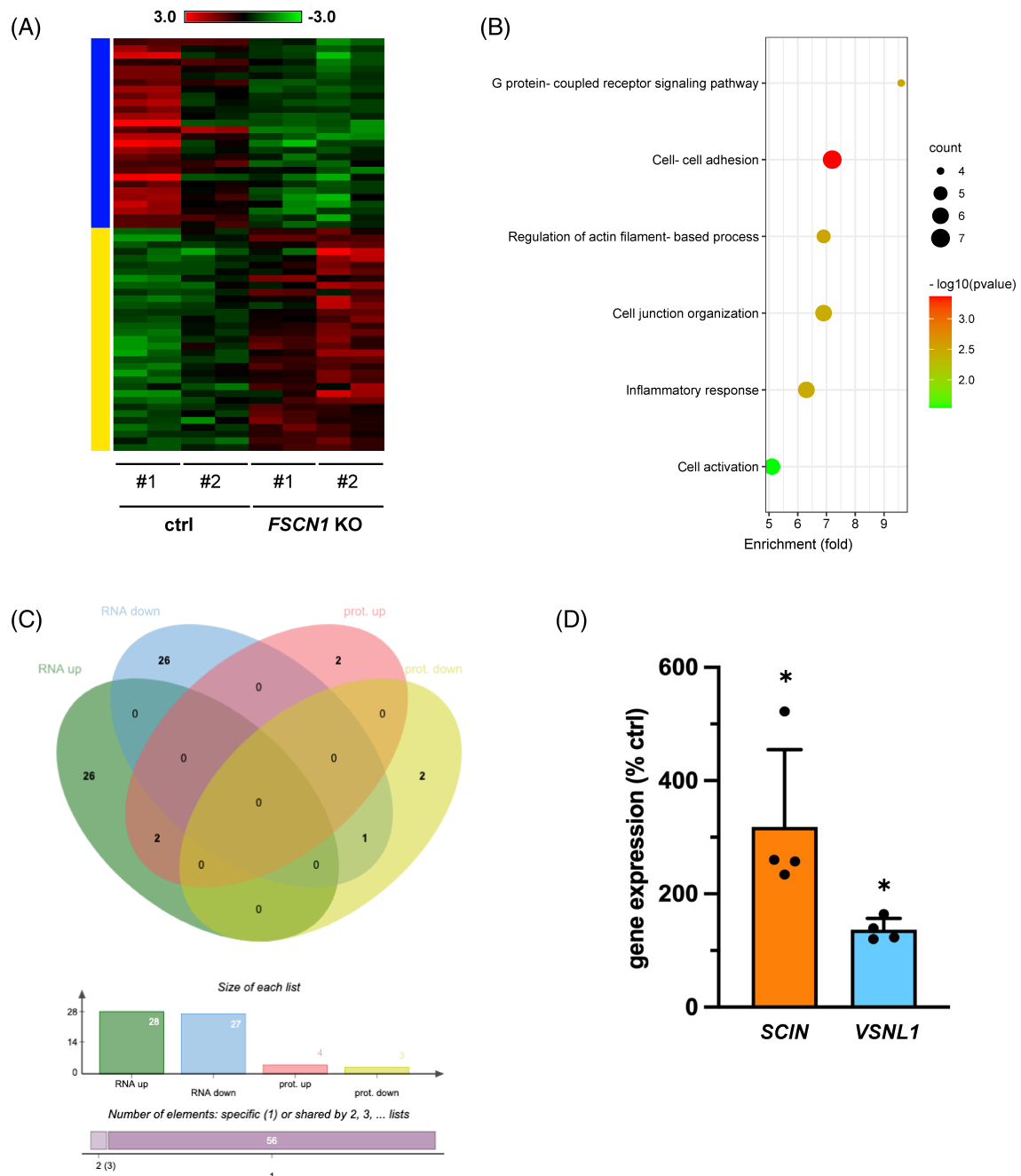


**FIGURE 3** Differences in gene and protein expression in *FSCN1* KO compared with ctrl H295R cells. (A) Heatmap of differentially expressed genes (DEG) in *FSCN1* KO cells compared with control cells. The yellow bar indicates genes upregulated, the blue bar genes downregulated in *FSCN1* KO cells, respectively. Log<sub>2</sub> scale is shown. (B) Gene Ontology (Biological Processes) categories enriched in DEG. (C) Intersection of the lists of transcripts and proteins found differentially regulated in *FSCN1* KO vs control cells. *SCIN* and *VSNL1* were upregulated at both the transcript and protein levels in *FSCN1* KO cells. (D) Transcript levels of *SCIN* and *VSNL1* measured by RT-qPCR in *FSCN1* KO and control H295R cells. *n* (independent experiments) = 4. Mean ± SD is shown. \**P* < .05, *t* test. [Color figure can be viewed at [wileyonlinelibrary.com](http://wileyonlinelibrary.com)]

develop an immune system until 14 days post fertilization, consequently human cells can survive and metastasize into zebrafish embryos. After injection into the subperidermal space of the yolk sac of zebrafish embryos, migration in the area of the animal tail was significantly reduced in *FSCN1* KO compared with control cells (Figure 5A-C; higher magnification images are shown in Figure S7).

Moreover, addition of the G2-044 compound to the waterbath, as shown in the diagram in Figure 5D, significantly reduced the number of metastases formed by ctrl cells (Figure 5E). All experiments were performed in the presence of Dox in the water bath to induce SF-1 overexpression and then increase the invasion capacities of H295R-derived cell clones.<sup>19,21</sup>

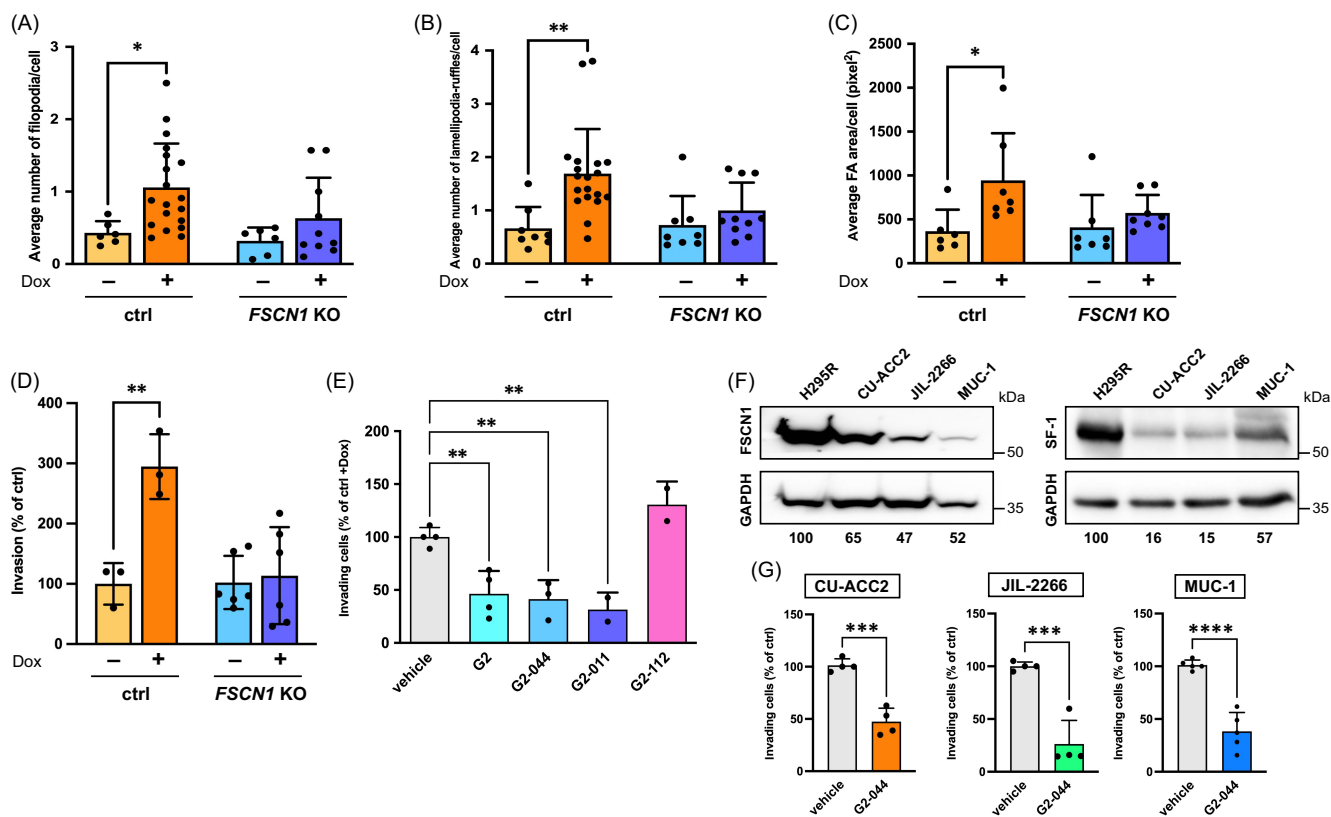


**FIGURE 4** FSCN1 inactivation or pharmacological inhibition reduces *in vitro* Matrigel invasion of ACC cells. Number of (A) filopodia, (B) lamellipodia/ruffles and (C) area of focal adhesions per cell in control and FSCN1 KO H295R cells treated with either vehicle or Dox (1  $\mu$ g/ml) for 24 h. *n* (independent experiments) = 6-9. Mean  $\pm$  SD is shown. \* $P$  < .05; \*\* $P$  < .01, one-way ANOVA with Šidák's multiple comparisons test. (D) *In vitro* Matrigel invasion of control and FSCN1 KO H295R cells treated with either vehicle or Dox (1  $\mu$ g/ml). Results are expressed as percentages of control cell invasion. *n* (independent experiments) = 3-6. Mean  $\pm$  SD is shown. \*\* $P$  < .01, one-way ANOVA with Šidák's multiple comparisons test. (E) *In vitro* Matrigel invasion of control H295R cells treated with Dox (1  $\mu$ g/ml) and with vehicle or G2 (50  $\mu$ M), G2-044, G2-011 or the inactive G2-112 compound (all 5  $\mu$ M). *n* (independent experiments) = 2-4. Mean  $\pm$  SD is shown. \*\* $P$  < .01, one-way ANOVA with Šidák's multiple comparisons test. (F) Left: immunoblot showing expression of FSCN1 and GAPDH in H295R, CU-ACC2, JIL-2266 and MUC-1 cells. FSCN1 levels (relative to GAPDH) in the CU-ACC2, JIL-2266 and MUC-1 ACC cell lines are indicated as percentages of H295R, which express the highest levels of FSCN1. Right: immunoblot showing expression of SF-1 and GAPDH in H295R, CU-ACC2, JIL-2266 and MUC-1 cells. SF-1 levels (relative to GAPDH) in the CU-ACC2, JIL-2266 and MUC-1 ACC cell lines are indicated as percentages of H295R, which express the highest levels of SF-1. FSCN1 and SF-1 band intensities were quantified by Image J after GAPDH normalization. *n* (independent experiments) = 3. (G) Matrigel invasion of those ACC cell lines treated with vehicle or G2-044 (5  $\mu$ M). *n* (independent experiments) = 4-5. Mean  $\pm$  SD is shown. \*\*\* $P$  < .001; \*\*\*\* $P$  < .0001, *t* test. [Color figure can be viewed at [wileyonlinelibrary.com](http://wileyonlinelibrary.com)]

## 4 | DISCUSSION

We have shown in this preclinical study that FSCN1 has an important role in regulating ACC cell invasion *in vitro* and in increasing their metastatic potential in an *in vivo* zebrafish model.

FSCN1 is a transcriptional target for  $\beta$ -catenin in H295R ACC cells, which express a constitutively active form of that protein. FSCN1 expression is significantly higher in CTNNB1 mutated tumors compared with the non-mutated ones and is positively correlated to CTNNB1 itself and with the levels of known  $\beta$ -catenin target genes in ACC,<sup>41</sup> suggesting common mechanisms of regulation. Upregulation of FSCN1 expression may represent an important mechanism by which adrenocortical cells harboring activating mutations in the Wnt/ $\beta$ -catenin pathway acquire a malignant phenotype.<sup>39</sup>

FSCN1 inactivation in H295R cells did not induce evident cytoskeletal alterations in basal culture conditions but significantly impaired cytoskeletal remodeling and Matrigel invasion induced by SF-1 upregulation in those cells. It is interesting to observe that FSCN1 KO induced differential expression of some genes involved in cell architecture and motility (Figure 3C), which suggests the presence of compensatory mechanisms in cells devoid of FSCN1. Recent studies have shown that FSCN1, in addition to its well-known function in the control of cytoskeletal dynamics, has broader roles in cancer cells favoring metastatic dissemination and target organ colonization.<sup>12</sup> Our FSCN1 KO ACC cells displayed proliferation defects, consistent with findings in other cancer types.<sup>44,45</sup> This phenotype may be related to the depletion of intracellular aspartate and glutamate in FSCN1 KO cells (Table S7), which are linked to purine and pyrimidine biosynthesis. Further studies are needed to elucidate the molecular

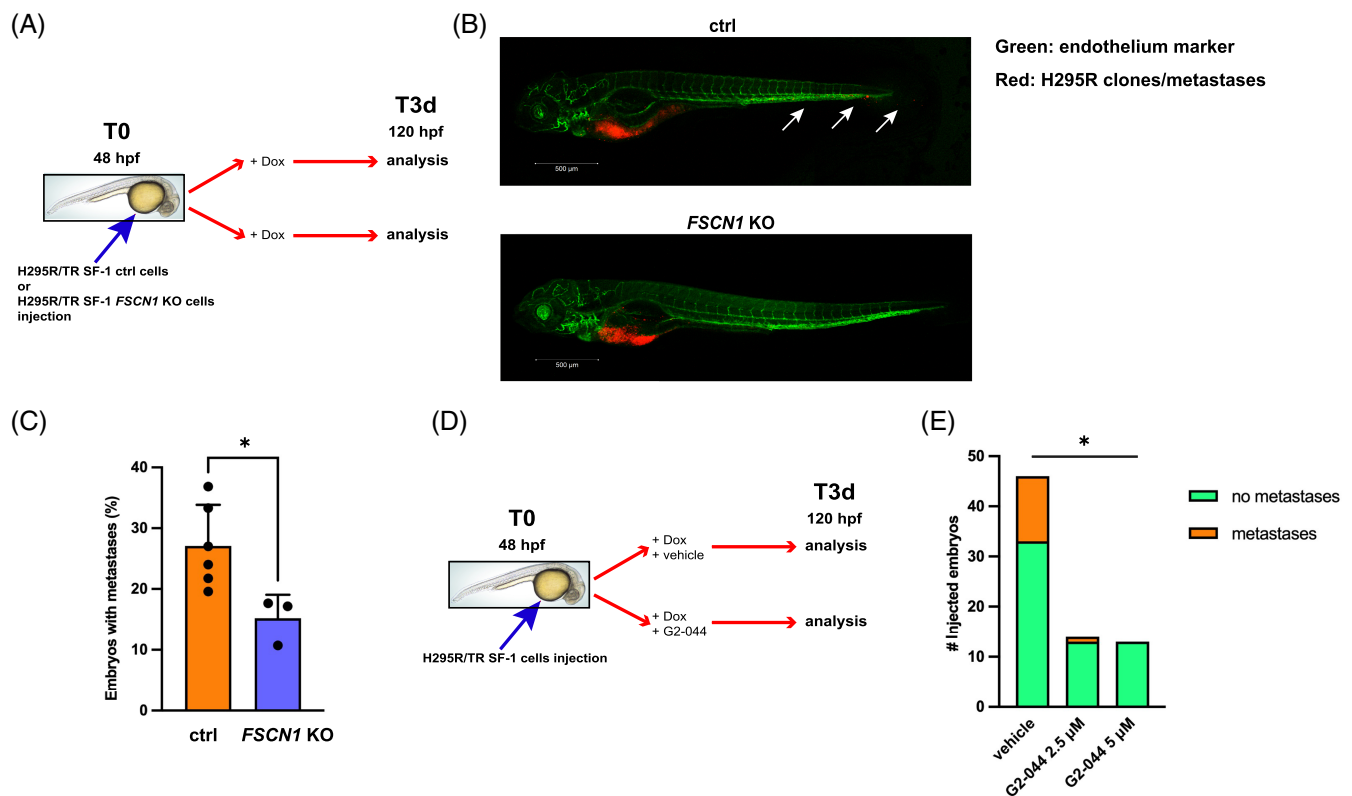


**FIGURE 5** FSCN1 inactivation or pharmacological inhibition reduces invasion in an *in vivo* zebrafish metastatic ACC model. (A) Diagram showing the plan of the zebrafish experiments involving ctrl and FSCN1 KO H295R/TR SF-1 clones. Dox-pretreated cells were injected in the yolk sac of 48 hpf zebrafish embryos and Dox (1  $\mu$ g/ml) was added to the water bath. Embryos were fixed and analyzed 3 days later at 120 hpf. (B) Representative lateral view images of Tg(kdr:EGFP) embryos at 120 hpf xenografted with H295R cells. Cells are labeled with a red fluorescent lipophilic dye while the embryos' endothelium is labeled with a green fluorescent protein reporter driven by the kdr promoter. Cells migrated in the caudal region of the zebrafish embryo are indicated by white arrows. Images were acquired using a Zeiss LSM 510 META confocal laser-scanning microscope at  $\times 10$  magnification. Top: control cells; bottom: FSCN1 KO cells. Scale bar, 500  $\mu$ m. Higher magnification images are shown in Figure S7. (C) Percentages of zebrafish embryos injected with control (orange) or FSCN1 KO H295R cells (blue) showing metastases in the presence of Dox (1  $\mu$ g/ml) in the bath to induce SF-1 overexpression.  $n$  (independent experiments) = 3-6, with 164 embryos in total injected with control cells; 97 embryos in total injected with FSCN1 KO cells. Mean  $\pm$  SD is shown. \* $P$  < .05, t test. (D) Diagram showing the plan of the zebrafish experiments aimed to study the effect of the G2-044 FSCN1 inhibitor on the metastatic activity of ctrl H295R/TR SF-1 cells. Dox-pretreated cells were injected in the yolk sac of 48 hpf zebrafish embryos and Dox (1  $\mu$ g/ml) was added to the water bath together with vehicle or G2-044. Embryos were fixed and analyzed 3 days later at 120 hpf. (E) Number of zebrafish embryos injected with ctrl H295R/TR SF-1 cells treated with vehicle, 2.5 and 5  $\mu$ M G2-044, respectively. Green, embryos without metastases; orange, embryos with metastases.  $n$  (independent experiments) = 2. \* $P$  < .05, chi-square. [Color figure can be viewed at [wileyonlinelibrary.com](http://wileyonlinelibrary.com)]

links between FSCN1 and regulation of cell proliferation in ACC cells. A limitation of this study is the absence of FSCN1 “put-back” experiments to confirm its function in FSCN1 KO cells. However, we believe that the data presented here are robust, since they were obtained by analysis of two different knock-out clones, where the presence of mutations in off-target genes produced by our CRISPR gene-inactivating strategy was thoroughly excluded, as described in section 2.3 and shown in Table S2. Moreover, FSCN1 “put-back” data were shown in our previous study,<sup>19</sup> which fully validated the results obtained after FSCN1 knock-down by siRNA. Another limitation is the lack of validation of most transcriptomic and proteomic results obtained. However, we focused on the two genes that were commonly found to be upregulated in FSCN1 KO cells both in transcriptomic and proteomic studies (SCIN and VSNL1) and validated the results obtained by RT-qPCR (Figure 3D). Furthermore, it has to be

underlined that metastasis is a multistep process including migration of the tumor cells from their primary site, dissemination in the circulatory system, colonization and survival in secondary sites.<sup>8</sup> The zebrafish model we employed to study the effects of FSCN1 gene inactivation or pharmacological antagonism on metastasis formation *in vivo* does not allow to discriminate among those different steps.

We have shown here that either FSCN1 gene inactivation or treatment with the specific FSCN1 inhibitor G2-044 inhibited H295R cell invasion in Matrigel and in an *in vivo* metastatic ACC model in zebrafish. Remarkably, the FSCN1 inhibitor also antagonized the invasion of other ACC cell lines which express lower levels of FSCN1 compared with H295R (Figure 4F). These data suggest that FSCN1 has an important function in the invasion process of ACC cell lines independently from its relative expression and that its inhibition may then be of therapeutic relevance even in cancers expressing low amounts of

this protein. G2-044 is an orally available FSCN1 inhibitor which has an improved potency compared with previous inhibitors.<sup>17</sup> A phase I clinical trial that employed this molecule showed efficacy in some patients with advanced, treatment-refractory solid cancers.<sup>46</sup> Another trial is presently ongoing to study the effect of G2-044 monotherapy or in combination with an anti-PD-(L)1-immune checkpoint inhibitor on metastatic cancers (NCT05023486). In addition to its direct involvement in the metastatic process, recent studies have highlighted the effects of FSCN1 on the antitumoural immune response. In the TCGA ACC cohort, *FSCN1* expression is negatively correlated with intratumoural effector and memory T cell signatures<sup>47</sup> and with PDL1 expression.<sup>48</sup> In our study, *FSCN1* KO in H295R cells strongly upregulated expression of *NLRP1*, a gene encoding a key protein in the inflammasome<sup>49</sup> (Table S5). In syngeneic mouse models of various cancers *FSCN1* inhibition by G2-044 synergized with immune checkpoint inhibitors and increased the numbers of intratumoural activated dendritic cells and activated CD8<sup>+</sup> T cells, leading to increased animal survival.<sup>50</sup> It is likely that the success of innovative therapies for ACC will be dependent on the combination of immunotherapies with treatments that counteract the immunosuppressive tumor microenvironment typical of those cancers.<sup>7</sup> Our study provides the rationale and preclinical data in support of testing the efficacy of *FSCN1* inhibitors in clinical trials including patients with ACC.

## AUTHOR CONTRIBUTIONS

The work reported in the paper has been performed by the authors, unless clearly specified in the text. Conceptualization: Enzo Lalli; methodology: Carmen Ruggiero, Mariangela Tamburello, Elisa Rossini, Silvia Zini, Nelly Durand, Giulia Cantini, Francesca Cioppi, Max Kurlbaum, Daniela Zizioli, Andrei Turtoi; provision of materials: Constanze Hantel, Katja Kiseljak-Vassiliades, Margaret E. Wierman, Laura-Sophie Landwehr, Isabel Weigand, Shengyu Yang; data analysis: Carmen Ruggiero, Mariangela Tamburello, Giulia Cantini, Francesca Cioppi, Max Kurlbaum, Andrei Turtoi, Michaela Luconi, Sandra Sigala, Enzo Lalli; supervision: Alfredo Berruti, Michaela Luconi, Sandra Sigala, Enzo Lalli; writing-original draft: Enzo Lalli; writing-review and editing: all authors.

## AFFILIATIONS

- <sup>1</sup>Institut de Pharmacologie Moléculaire et Cellulaire CNRS UMR 7275, 06560 Valbonne, France
- <sup>2</sup>Université Côte d'Azur, 06560 Valbonne, France
- <sup>3</sup>Section of Pharmacology, Department of Molecular and Translational Medicine, University of Brescia, 25124 Brescia, Italy
- <sup>4</sup>Endocrinology Unit, Department of Experimental and Clinical Biomedical Sciences "Mario Serio", University of Florence, 50134 Florence, Italy
- <sup>5</sup>Centro di Ricerca e Innovazione sulle Patologie Surrenaliche, AOU Careggi, 50134 Florence, Italy
- <sup>6</sup>Department of Experimental and Clinical Medicine, University of Florence, 50134 Florence, Italy
- <sup>7</sup>Department of Endocrinology, Diabetology and Clinical Nutrition, University Hospital Zurich (USZ) and University of Zurich (UZH), 8091 Zürich, Switzerland

<sup>8</sup>Medizinische Klinik und Poliklinik III, University Hospital Carl Gustav Carus Dresden, 01307 Dresden, Germany

<sup>9</sup>Division of Endocrinology, Metabolism and Diabetes, Department of Medicine, University of Colorado Anschutz Medical Campus, 80045 Aurora, Colorado, USA

<sup>10</sup>Rocky Mountain Regional Veterans Affairs Medical Center, 80045 Aurora, Colorado, USA

<sup>11</sup>Division of Endocrinology and Diabetology—Department of Internal Medicine I, University Hospital, University of Würzburg, 97080 Würzburg, Germany

<sup>12</sup>Department of Medicine IV, University Hospital Munich, Ludwig-Maximilians-Universität München, 81377 Munich, Germany

<sup>13</sup>Section of Biotechnology, Department of Molecular and Translational Medicine, University of Brescia, 25124 Brescia, Italy

<sup>14</sup>Tumor Microenvironment and Resistance to Therapy Laboratory, Institut de Recherche en Cancérologie de Montpellier, Université de Montpellier-INSERM U1194, 34090 Montpellier, France

<sup>15</sup>Platform for Translational Oncometabolomics, Biocampus, CNRS-INSERM-Université de Montpellier, 34090 Montpellier, France

<sup>16</sup>Department of Cellular and Molecular Physiology, Penn State University College of Medicine, 17033 Hershey, Pennsylvania, USA

<sup>17</sup>Oncology Unit, Department of Medical and Surgical Specialties, Radiological Sciences and Public Health, University of Brescia and ASST Spedali Civili di Brescia, 25123 Brescia, Italy

<sup>18</sup>Inserm, 06560 Valbonne, France

## ACKNOWLEDGEMENTS

sgCtr-LentiCRISPRv2 was a gift from William Kaelin (Addgene plasmid #107402). We thank D. Vignjevic (Institut Curie, Paris, France) for providing the *FSCN1* promoter-luciferase reporter and the  $\Delta$ N-TCF4 expression plasmids; F. Luton (IPMC, Valbonne, France) for the gift of the anti-paxillin antibody; E. Pallesi-Pocachard (Molecular and Cellular Biology Platform, INMED Marseille, France) for DNA sequencing; J. Cazareth (IPMC, Valbonne, France) for flow cytometric analysis; M. Decourcelle (Functional Proteomics Platform of the Montpellier Proteomics Platform, BioCampus Montpellier, France) for proteomic analysis; E. Turtoi (PLATON platform, MAMMA facility, UAR Biocampus Montpellier, France) for metabolite analysis.

## FUNDING INFORMATION

This study was supported by the Fondation ARC Project PJA 20191209289 grant to Carmen Ruggiero and ANR20-CE14-0007 (Goldilocks) grant to Enzo Lalli. The Orbitrap Exploris 480 mass spectrometer used at the Montpellier Proteomics Platform (PPM, BioCampus) for proteomics analysis was co-financed by the European Regional Development Fund (ERDF) and the Occitanie region. Andrei Turtoi is supported by a LabEx MablImprove Starting Grant and SIRIC Montpellier Cancer Grant INCa\_Inserm\_DGOS\_12553. The equipment of the Platform for Translational Oncometabolomics, Biocampus Montpellier, is funded by the French Ministry for Higher Education and Research through a CPER grant (IBDLR).

## CONFLICT OF INTEREST STATEMENT

The authors declare no conflicts of interest.

## DATA AVAILABILITY STATEMENT

Anonymized clinical and genetic data of patients with ACC are publicly available in the Xena Functional Genomics (<https://xenabrowser.net>) and cBioportal (<https://www.cbioportal.org>) websites. RNA-seq data are available as GSE216008 in Gene Expression Omnibus (<https://www.ncbi.nlm.nih.gov/geo>). The raw mass spectrometry proteomics data have been deposited in the ProteomeXchange Consortium via the MassIVE partner repository (<https://massive.ucsd.edu/>) with the database identifier MSV000090738. The raw metabolomics data have been deposited to the EMBL-EBI MetaboLights database with the identifier MTBLS6402. Other data that support the findings of this study are available from the corresponding authors upon request.

## ETHICS STATEMENT

All patients with ACC in the Florence cohort gave their written informed consent to the study, which was approved by the local ethical committee (Prot.2017-277 BIO 59/11, September 27, 2017). Zebrafish were maintained and used according to EU Directive 2010/63/EU for animal use following protocols approved by the local committee (OPBA) and authorized by the Italian Ministry of Health (authorization number 393/2017).

## ORCID

Michaela Luconi  <https://orcid.org/0000-0001-5186-064X>

Enzo Lalli  <https://orcid.org/0000-0002-0584-5681>

## REFERENCES

- Valastyan S, Weinberg RA. Tumor metastasis: molecular insights and evolving paradigms. *Cell*. 2011;147:275-292.
- Vanharanta S, Massagué J. Origin of metastatic traits. *Cancer Cell*. 2013;24:410-421.
- Fontebasso Y, Dubinett SM. Drug development for metastasis prevention. *Crit Rev Oncog*. 2015;20:449-473.
- Lalli E, Luconi M. The next step: mechanisms driving adrenocortical carcinoma metastasis. *Endocr Relat Cancer*. 2018;25:R31-R48.
- Terzolo M, Angeli A, Fassnacht M, et al. Adjuvant mitotane treatment for adrenocortical carcinoma. *N Engl J Med*. 2007;356:2372-2380.
- Fassnacht M, Terzolo M, Allolio B, et al. Combination chemotherapy in advanced adrenocortical carcinoma. *N Engl J Med*. 2012;366:2189-2197.
- Grisanti S, Cosentini D, Laganà M, et al. The long and winding road to effective immunotherapy in patients with adrenocortical carcinoma. *Future Oncol*. 2020;16:3017-3020.
- Ruggiero C, Lalli E. Targeting the cytoskeleton against metastatic dissemination. *Cancer Metastasis Rev*. 2021;40:89-140.
- Jayo A, Parsons M, Adams JC. A novel Rho-dependent pathway that drives interaction of fascin-1 with p-Lin-11/Isl-1/Mec-3 kinase (LIMK) 1/2 to promote fascin-1/actin binding and filopodia stability. *BMC Biol*. 2012;10:72.
- Johnson HE, King SJ, Asokan SB, Rotty JD, Bear JE, Haugh JM. Fascin bundles direct the initiation and orientation of lamellipodia through adhesion-based signaling. *J Cell Biol*. 2015;208:443-455.
- Hashimoto Y, Kim DJ, Adams JC. The roles of fascin in health and disease. *J Pathol*. 2011;224:289-300.
- Lin S, Taylor MD, Singh PK, Yang S. How does fascin promote cancer metastasis? *FEBS J*. 2021;288:1434-1446.
- Kulasingham V, Diamandis EP. Fascin-1 is a novel biomarker of aggressiveness in some carcinomas. *BMC Med*. 2013;11:53.
- Tan VY, Lewis SJ, Adams JC, Martin RM. Association of fascin-1 with mortality, disease progression and metastasis in carcinomas: a systematic review and meta-analysis. *BMC Med*. 2013;11:52.
- Chen L, Yang S, Jakoncic J, Zhang JJ, Huang XY. Migrastatin analogues target fascin to block tumour metastasis. *Nature*. 2010;464:1062-1066.
- Huang FK, Han S, Xing B, et al. Targeted inhibition of fascin function blocks tumour invasion and metastatic colonization. *Nat Commun*. 2015;6:7465.
- Han S, Huang J, Liu B, et al. Improving fascin inhibitors to block tumor cell migration and metastasis. *Mol Oncol*. 2016;10:966-980.
- Poli G, Ceni E, Armignacco R, et al. 2D-DIGE proteomic analysis identifies new potential therapeutic targets for adrenocortical carcinoma. *Oncotarget*. 2015;6:5695-5706.
- Poli G, Ruggiero C, Cantini G, et al. Fascin-1 is a novel prognostic biomarker associated with tumor invasiveness in adrenocortical carcinoma. *J Clin Endocrinol Metab*. 2019;104:1712-1724.
- Cantini G, Fei L, Canu L, et al. Circulating Fascin 1 as a promising prognostic marker in adrenocortical cancer. *Front Endocrinol*. 2021;12:698862.
- Ruggiero C, Doghman-Bouguerra M, Sbiera S, et al. Dosage-dependent regulation of VAV2 expression by steroidogenic factor-1 drives adrenocortical carcinoma cell invasion. *Sci Signal*. 2017;10:eal2464.
- Fassnacht M, Johanssen S, Quinkler M, et al. International Union against Cancer staging classification for adrenocortical carcinoma: proposal for a revised TNM classification. *Cancer*. 2009;115:243-250.
- Hantel C, Shapiro I, Poli G, et al. Targeting heterogeneity of adrenocortical carcinoma: evaluation and extension of preclinical tumor models to improve clinical translation. *Oncotarget*. 2016;7:79292-79304.
- Kiseljak-Vassiliades K, Zhang Y, Bagby SM, et al. Development of new preclinical models to advance adrenocortical carcinoma research. *Endocr Relat Cancer*. 2018;25:437-451.
- Landwehr LS, Schreiner J, Appenzeller S, et al. A novel patient-derived cell line of adrenocortical carcinoma shows a pathogenic role of germline MUTYH mutation and high tumour mutational burden. *Eur J Endocrinol*. 2021;184:823-835.
- Lin S, Huang C, Gunda V, et al. Fascin controls metastatic colonization and mitochondrial oxidative phosphorylation by remodeling mitochondrial Actin filaments. *Cell Rep*. 2019;228:2824-2836.e8.
- Gao W, Li W, Xiao T, Liu XS, Kaelin WG Jr. Inactivation of the PBRM1 tumor suppressor gene amplifies the HIF-response in VHL-/- clear cell renal carcinoma. *Proc Natl Acad Sci U S A*. 2017;114:1027-1032.
- Villari G, Jayo A, Zanet J, et al. A direct interaction between fascin and microtubules contributes to adhesion dynamics and cell migration. *J Cell Sci*. 2015;128:4601-4614.
- Leal LF, Bueno AC, Gomes DC, Abduch R, de Castro M, Antonini SR. Inhibition of the Tcf/beta-catenin complex increases apoptosis and impairs adrenocortical tumor cell proliferation and adrenal steroidogenesis. *Oncotarget*. 2015;6:43016-43032.
- Livak KJ, Schmittgen TD. Analysis of relative gene expression data using real-time quantitative PCR and the  $2^{-\Delta\Delta CT}$  method. *Methods*. 2001;25:402-408.
- Vignjevic D, Schoumacher M, Gavert N, et al. Fascin, a novel target of beta-catenin-TCF signaling, is expressed at the invasive front of human colon cancer. *Cancer Res*. 2007;67:6844-6853.

32. Kurlbaum M, Sbierra S, Kendl S, Fassnacht M, Kroiss M. Steroidogenesis in the NCI-H295 cell line model is strongly affected by culture conditions and substrain. *Exp Clin Endocrinol Diabetes*. 2020;128:672-680.
33. Jalili V, Afgan E, Gu Q, et al. The galaxy platform for accessible, reproducible and collaborative biomedical analyses: 2020 update. *Nucleic Acids Res*. 2020;48:W395-W402.
34. Zhou Y, Zhou B, Pache L, et al. Metascape provides a biologist-oriented resource for the analysis of systems-level datasets. *Nat Commun*. 2019;10:1523.
35. Bardou P, Mariette J, Escudié F, Djemiel C, Klopp C. jvenn: an interactive Venn diagram viewer. *BMC Bioinformatics*. 2014;15:293.
36. Basnet RM, Zizioli D, Muscò A, et al. Caffeine inhibits direct and indirect angiogenesis in zebrafish embryos. *Int J Mol Sci*. 2021;22:4856.
37. Gianoncelli A, Guarienti M, Fragni M, et al. Adrenocortical carcinoma xenograft in zebrafish embryos as a model to study the *in vivo* cytotoxicity of abiraterone acetate. *Endocrinology*. 2019;60:2620-2629.
38. Lippert J, Appenzeller S, Liang R, et al. Targeted molecular analysis in adrenocortical carcinomas: a strategy toward improved personalized prognostication. *J Clin Endocrinol Metab*. 2018;103:4511-4523.
39. Gaujoux S, Grabar S, Fassnacht M, et al.  $\beta$ -Catenin activation is associated with specific clinical and pathologic characteristics and a poor outcome in adrenocortical carcinoma. *Clin Cancer Res*. 2011;17:328-336.
40. Sigala S, Bothou C, Penton D, et al. A comprehensive investigation of steroidogenic signaling in classical and new experimental cell models of adrenocortical carcinoma. *Cell*. 2022;11:1439.
41. Lefèvre L, Omeiri H, Drougat L, et al. Combined transcriptome studies identify *AFF3* as a mediator of the oncogenic effects of  $\beta$ -catenin in adrenocortical carcinoma. *Oncogenesis*. 2015;4:e161.
42. Sewer MB, Li D. Regulation of adrenocortical steroid hormone production by RhoA-diaphanous 1 signaling and the cytoskeleton. *Mol Cell Endocrinol*. 2013;371:79-86.
43. Relav L, Doghman-Bouguerra M, Ruggiero C, Muzzi JCD, Figueiredo B, Lalli E. Steroidogenic factor 1, a goldilocks transcription factor from adrenocortical organogenesis to malignancy. *Int J Mol Sci*. 2023;24:3585.
44. Fu H, Wen JF, Hu ZL, Luo GQ, Ren HZ. Knockdown of *fascin1* expression suppresses the proliferation and metastasis of gastric cancer cells. *Pathology*. 2009;41:655-660.
45. Park SH, Song JY, Kim YK, et al. *Fascin1* expression in high-grade serous ovarian carcinoma is a prognostic marker and knockdown of *fascin1* suppresses the proliferation of ovarian cancer cells. *Int J Oncol*. 2014;44:637-646.
46. Chung V, Jhaveri KL, Hoff DDV, et al. Phase 1A clinical trial of the first-in-class *fascin* inhibitor NP-G2-044 evaluating safety and anti-tumor activity in patients with advanced and metastatic solid tumors. *J Clin Oncol*. 2021;39:2548.
47. Liang J, Liu Z, Wei X, et al. Expression of *FSCN1* and *FOXM1* are associated with poor prognosis of adrenocortical carcinoma patients. *BMC Cancer*. 2019;19:1165.
48. Billon E, Finetti P, Bertucci A, et al. *PDL1* expression is associated with longer postoperative survival in adrenocortical carcinoma. *Oncoimmunology*. 2019;8:e1655362.
49. Taabazuig CY, Griswold AR, Bachovchin DA. The *NLRP1* and *CARD8* inflammasomes. *Immunol Rev*. 2020;297:13-25.
50. Wang Y, Song M, Liu M, et al. *Fascin* inhibitor increases intratumoral dendritic cell activation and anti-cancer immunity. *Cell Rep*. 2021;35:108948.

#### SUPPORTING INFORMATION

Additional supporting information can be found online in the Supporting Information section at the end of this article.

**How to cite this article:** Ruggiero C, Tamburello M, Rossini E, et al. *FSCN1* as a new druggable target in adrenocortical carcinoma. *Int J Cancer*. 2023;1-14. doi:10.1002/ijc.34526